Article

Combined Metabonomic and Quantitative Real-Time PCR Analyses Reveal Systems Metabolic Changes in Jurkat T-cells Treated with HIV-1 Tat Protein

Wenting Liao, Guangguo Tan, Zhen Yu Zhu, Qiuli Chen, Ziyang Lou, Xin Dong, Wei Zhang, Wei Pan, and Yifeng Chai

J. Proteome Res., **Just Accepted Manuscript** • Publication Date (Web): 02 Oct 2012

Title page

Article title: Combined Metabonomic and Quantitative Real-Time PCR Analyses Reveal Systems Metabolic Changes in Jurkat T-cells Treated with HIV-1 Tat Protein

Running title: Systems Metabolic Changes in Jurkat T-cells Treated with Tat

Keywords: HIV-1 Tat protein, metabonomics, GC-MS, RPLC-MS, HILIC-MS, quantitative real-time PCR

Author

Wenting Liao,[†,§,ıı] Guangguo Tan, [†, ıı] Zhenyu Zhu,[†] Qiuli Chen,[‡] Ziyang Lou,[†] Xin Dong, [†] Wei Zhang,[†] Wei Pan, [‡, *] and Yifeng Chai [†, *]

School of Pharmacy, Second Military Medical University, Shanghai 200433, China, Department of Microbiology, Second Military Medical University, Shanghai 200433, China, College of High Altitude Military Medicine, Third Military Medical University, Chongqing 400038, China

* To whom correspondence should be addressed. E-mail: yfchai@smmu.edu.cn Tel.: +86-21-8187-1201, Fax: +86-21-8187-1201 for Yifeng chai and E-mail: pwpanwei@yahoo.com.cn Tel.:+86 21 81870989, Fax: +86 21 81870989 for Wei Pan.

[†] School of Pharmacy, Second Military Medical University.

[‡] Department of Microbiology, Second Military Medical University.

[§] College of High Altitude Military Medicine, Third Military Medical University

[ıı] Authors with equal contribution to the research.

Abstract

HIV-1 Tat protein is released by infected cells and can affect bystander uninfected T cells and induce numerous biological responses which contribute to its pathogenesis. To elucidate the complex pathogenic mechanism, we conducted a comprehensive investigation on Tat protein-related extracellular and intracellular metabolic changes in Jurkat T-cells using combined gas chromatography-mass spectrometry (GC-MS), reversed-phase liquid chromatography-mass spectrometry (RPLC-MS) and a hydrophilic interaction liquid chromatography-mass spectrometry (HILIC-MS)-based metabonomics approach. Quantitative real-time PCR (qRT-PCR) analyses were further employed to measure expressions of several relevant enzymes together with perturbed metabolic pathways. Combined metabonomic and qRT-PCR analyses revealed that HIV-1 Tat caused significant and comprehensive metabolic changes, as represented by significant changes of 37 metabolites and 10 relevant enzymes in HIV-1 Tat-treated cells. Using MetaboAnalyst 2.0, it was found that eleven pathways (Impact-value > 0.10) among the regulated pathways were acutely perturbed, including sphingolipid metabolism, glycine, serine and threonine metabolism, pyruvate metabolism, inositol phosphate metabolism, arginine and proline metabolism, citrate cycle, phenylalanine metabolism, tryptophan metabolism, pentose phosphate pathway, glycerophospholipid metabolism, glycolysis or gluconeogenesis. These results provide metabolic evidence of the complex pathogenic mechanism of HIV-1 Tat

protein as a “viral toxin”, and would help obligate Tat protein as “an important target” for therapeutic intervention and vaccine development.

Keywords: HIV-1 Tat protein, metabonomics, GC-MS, RPLC-MS, HILIC-MS, quantitative real-time PCR

Introduction

HIV-1 infection is characterized by early viremia followed by a long period of clinical latency in which the level of virus production reflects a continuous process of new infection at a rate that balances the rapid death of productively infected cells. After years, when a clinically apparent disease develops, this steady state is unbalanced toward an exponential increase in viral burden. During all these steps, infected cells release soluble factors that likely contribute to the infectivity of nearby uninfected cells [1].

HIV-1 transactivator of transcription Tat, although known as a nuclear factor, is released by infected cells both *in vitro* and *in vivo* and has numerous biological activities that might contribute either to the impairment of the immune response or to viral dissemination and pathogenesis. Extracellular Tat, secreted from infected cells, was found to play an important role in the pathogenesis of AIDS associated Kaposi's sarcoma (KS), HIV-1 associated dementia and apoptosis of $CD4^+$ T cells by both direct interacting with the membrane receptors or intracellular regulatory elements of target cells and bystanding effects of induced cytokines [2]. Secreted Tat can induce apoptosis in neighboring uninfected cells [3, 4], inhibit the proliferation of uninfected T-cells [3, 4], and upregulate the expression of HIV-1 coreceptor CXC chemokine receptor-4 on T-lymphocytes [5, 6], rendering bystander $CD4^+$ T cells more susceptible to HIV-1 infection. These findings support the notion that Tat acts as a viral “toxin” [7], and obligate it as “an important target” for drug intervention

and therapeutic vaccines. Indeed, some promising therapeutic effects were observed in phase II trial of Tat vaccine [8, 9].

A number of chronic metabolic abnormalities including disorders of lipid metabolism with or without lipodystrophy [10], insulin resistance [11], cardiometabolic syndrome [11], altered phosphate metabolism [12], and an increased prevalence of impaired glucose tolerance [13] are found prevalent in HIV patients with or without receiving highly active antiretroviral therapy (HAART). Although multiple risk factors have been proposed, the etiology of these metabolic abnormalities remains unclear. It would be interesting to see whether HIV-1 Tat plays a critical role in HIV metabolic abnormalities.

Metabonomics is a top-down systems biology approach whereby metabolic responses to biological interventions or environmental factors are analyzed and modeled [14]. Metabonomics provides insights into the global metabolic status of the entire organism by monitoring the entire pattern of low molecular weight compounds rather than focusing on an individual metabolic intermediate (MI). It has shown great promise in the elucidation of highly complex metabolic outcomes induced by viral infections at steady state levels [15, 16]. An extensive metabonomics study needs non-discriminatory analytical techniques with each analytical instrument being selective to certain metabolites, and therefore parallel use of multiple analytical methods would be advantageous in identifying a broader spectrum of metabolites relevant to physiopathological alteration [17-19].

We previously reported that HIV-1 Tat induced multiple metabolic changes involving glycolysis, citrate cycle, fatty acid metabolism and amino acid metabolism in mice based on the gas chromatography–mass spectrometry (GC-MS)-based metabonomic approach [20]. In this study, we systematically investigated metabolic changes in Jurkat cell line induced by Tat protein using GC-MS, reversed-phase liquid chromatography–mass spectrometry (RPLC-MS) and hydrophilic interaction liquid chromatography-mass spectrometry (HILIC-MS)-based metabonomic methods. The metabolite network of Tat-treated Jurkat T-cells was predicted via MetaboAnalyst 2.0. Quantitative real-time PCR (qRT-PCR) analyses were further employed to measure expressions of ten relevant genes together with perturbed metabolic pathways found by metabonomic analysis. The objectives of this study are to determine how HIV-1 Tat influences cellular metabolic environments in uninfected $CD4^+$ T cells as the important target for extracellular Tat protein. Our data presented here together with the previous findings seem to suggest that Tat could be an important etiologic factor for HIV-related metabolic abnormalities.

Materials and Methods

The schematic flowchart of the metabolic profiling strategy used in this study is illustrated in Figure 1.

Reagents

Formic acid was obtained from Fluka (Buchs, Switzerland). Methoxylamine hydrochloride, N-methyl-N-(trimethylsilyl)-trifluoracetamide (MSTFA), pyridine, trimethyl-chlorosilane (TMCS), ammonium formate, and citrate were purchased from Sigma-Aldrich (St. Louis, MO, USA). Methanol and acetonitrile (ACN) are chromatography pure (Merck, Germany). Lysophosphatidylcholine(16:0) Lysophosphatidylcholine (18:0), and Lysophosphatidylcholine (18:1) were purchased from Larodan AB (Malmö, Sweden). Sphinganine was purchased from Acros Organics (NewJersey, USA). Lactate, L-alanine, sodium succinate, malic acid, L-proline, phenylalanine, L-valine, isoleucine, palmitinic acid, stearic acid, glucose and cholesterol were obtained from Shanghai Jingchun Reagent Co., Ltd.

Recombinant HIV-1 Clade B Tat Protein

Endotoxin-free recombinant HIV-1 Clade B Tat Protein was purchased from Diatheva (Fano, Italy). According to the manufacturer's data sheet, the purity of the Tat protein was over 90%, with preserved biological activity. To prevent oxidation and loss of biological activity, the Tat protein was lyophilized and stored at −80 ℃, reconstituted in sterile degassed PBS before use, and handled as described [21]. This Tat protein was heat-inactivated by incubation at 85℃ for 30 min as previously described [22]. The heat-inactivated Tat protein (inaTat) has been extensively used as a negative control for bioactive Tat [22-24]

and was used as a control for the Tat-induced biochemical changes in this study.

Assessment of Cell Proliferation by MTT Assay

Jurkat cell line was purchased from the Cell Bank of Shanghai Institutes for Biological Sciences and cultured in RPMI1640 supplemented with 10% FBS, 100 U/mL penicillin and 100 U/mL streptomycin. Cells were maintained at 37 ℃ in an atmosphere of 5% CO_2. The proliferation of Jurkat cells was assessed using the 3-(4,5-dimethylthiazol-2-yl)-2,5-diphenyltetrazolium bromide (MTT) reduction assay. In the MTT assay, the yellow tetrazolium salt (MTT) is reduced in metabolically active cells to form insoluble purple formazan crystals, which are solubilized by the addition of a detergent. The color can then be quantitated by spectrophotometry. Continuously growing Jurkat T cells were seeded at 10^6 cells/ml in a 96-well plate and were incubated with Tat protein at a final concentration of 10 nM, 50 nM or 100 nM for 24 or 48 h, and further incubated with 20 μl MTT solution (5 mg/ml; Sigma-Aldrich) for 4 h at 37 ℃. Cells were centrifuged at 800 rpm for 10 min, and then 150 μl DMSO was added and mixed by gentle pipetting to solubilize the cells. The optical density of the solution was read at 570 nm using a Universal Microplate Reader (Bio-Tek Instruments, Inc.). Subsequently, the inhibition rate of Jurkat cells was calculated according to the absorbance of treated cells and control cells.

Determination of Apoptosis by Fow Cytometry

Jurkat cells were treated in the same way as described above, and the percentage of apoptotic cells was determined by flow cytometry using an FITC annexin V Apoptosis Detection Kit (BD Pharmingen, SanDiego, CA, USA) according to the manufacturer's protocol as previously described [25]. In brief, 10^5 cells/sample were washed with PBS and then resuspended in 100 µl binding buffer containing 5 µl FITC-annexin V and 10 µl propidium iodide and incubated at room temperature for 15 min. Then, 400 µl binding buffer was added, and cells were analyzed in a FACSCalibur flow cytometer (Becton-Dickinson, San Jose, CA, USA). Cells were gated for lymphocytes using forward and side scatter. Ten thousand events were recorded from each treatment group. The samples were analyzed using Becton-Dickinson CellQuest and WinMDI 2.8 (Windows Multiple Document Interface for Flow Cytometry) software.

Cell Experiments

Jurkat T-cells were seeded at 10^6 cells/ml into a 10 cm dish and treated with bioactive Tat or inaTat protein at a final concentration of 100 nM or an equal volume of vehicle (PBS) as a control. This concentration of Tat was based on the above-mentioned MTT and apoptosis assays. After 48 h, cells were counted using a hemocytometer (Neubauer chamber) and cell suspension (10 ml) was quenched by pouring into tubes containing 40 ml cold

0.9% (w/v) NaCl (0.5 ℃) [26]. Cells were harvested by centrifuging at 1200 rpm for 5 min and snap frozen in liquid nitrogen. The supernatant samples were collected and immediately frozen in liquid nitrogen. Five independent biological replicates (i.e. tissue culture dishes) were examined in each group.

Metabonomic Analysis

GC-MS Sample Preparation

The extraction of intracellular metabolites from Jurkat cells was performed as previously described [16]. In brief, cell pellets were dissolved in a mixture of chloroform/methanol/water at a ratio of 2:5:2 (v/v/v). The samples were ultrasonicated in an ice bath ultra-sonicator for 30 min and subsequently centrifuged at 18000 g for 10 min at 4 ℃. 1.6 mL supernatant was collected and divided into two aliquots (one for GC-MS analysis and the other for LC-MS analysis) and dried with a gentle nitrogen stream. The supernatant sample (1 mL) was lyophilized. Immediately prior to GC-MS analysis, derivatization was performed in two steps: Firstly, methoximation was carried out by dissolving the sample in 50 µL solution of methoxyamine hydrochloride (20 mg/mL) in pyridine to protect the carbonyls. The incubation was kept at 37 ℃ for 60 min. Silylation was then carried out by adding 50 µL MSTFA with 1% TMCS to each sample for 30 min at 70 ℃.

GC-MS Analysis

The derivatized samples for GC-MS were analyzed on a Thermo-Finnigan Trace DSQ fasting scanning single-quadrupole MS (Thermo Electron Corporation) operated at unit mass resolving power. 0.5 µL sample solution was injected in a splitless mode to a TR-5MS column (30m×250µm×0.25µm) with helium as the carrier gas at a flow of 1 ml/min. The injector temperature was set at 260 ℃. The temperature of the ion source was adjusted to 200 ℃ and that of quadrupole was set at 150 ℃. GC-MS was operated using electron impact ionization with a 60-600 atomic mass unit (amu) scan range. The initial temperature of the column was kept at 70 ℃ for 3 min. Then, the temperature was ramped at 4 ℃ / min to 220 ℃ and then to 310 ℃ at a rate of 12 ℃ / min where it was held for 10 min. To reduce systematic error associated with instrument drift, samples were run in an order that alternated among the Tat-treated group, inaTat-treated group and the control group. Each sample was run in duplicate, and after data integration, duplicate runs were averaged. An in-house quality control (QC) was prepared by pooling and mixing the same volume of each sample [27].

LC-MS Sample Preparation

The dried cell extracts was resuspended in 100 µL ACN/water solution (7:3, v/v) and liquid transferred to a 1.5 ml centrifuge tube. The tubes were centrifuged at 18000 g for 10 min at 4 ℃ and 75 µL supernatant was transferred to an LC-MS vial. An in-house QC was prepared by pooling and

mixing the same volume of each sample.

To prepare medium samples for LC-MS analysis, 1 mL lyophilized culture medium was resuspended in 150 µL ACN/water solution (7:3, v/v). The tubes were centrifuged at 18000 g for 10 min at 4 ℃ and 75 µL supernatant was removed for LC-MS analysis. An in-house QC was prepared by pooling and mixing the same volume of each sample.

LC-MS Analysis

Chromatography was performed on Agilent 1290 Infinity LC system. The column oven was set at 40 ℃. An acquity UPLC BEH C_{18} column (2.1 mm × 100 mm, 1.7 µm, Waters, Milford, MA) was used for reversed phase separation. The mobile phase consisted of 0.1% formic acid (A) and ACN modified with 0.1% formic acid (B), using a gradient elution of 5% B at 0–3 min, 5%–95% B at 3–23 min, 95% B at 23–25 min. The total run time was 30 min including equilibration. The flow rate was 350 µL/min and the injection volume was 4 µL.

For HILIC analysis, an acquity UPLC BEH HILIC C_{18} column (2.1 mm × 100 mm, 1.7 µm, Waters, Milford, MA) was used on the same LC system as above. The mobile phase consisted of 10 mM ammonium formate modified with 0.1% formic acid (A) and ACN modified with 0.1% formic acid (B), using a gradient elution of 95%B at 0–10 min, 95%–90% B at 10–14 min, 90% B at 14–24 min, 90%–60% B at 24–28 min, 60% B at 28-30 min. The total run time

was 35 min including equilibration. The flow rate was 350 µL/min and the injection volume was 4 µL.

Mass spectrometric analyses were performed with an Agilent 6530 Accurate-Mass Quadrupole Time-of-Flight (Q-TOF) mass spectrometer (Agilent, USA) with mass spectrometry parameters as previously described [28]. The Q-TOF mass spectrometer was operated in a positive ion mode with a capillary voltage of 3.5 kV, drying gas flow of 11 L/min, and a gas temperature of 350 ℃. The nebulizer pressure was set at 45 psig. The fragmentor voltage was set at 120 V and skimmer voltage was set at 60 V. All analyses were acquired using a mixture of 10 mM purine (m/z 121.0508) and 2 mM hexakis phosphazine (m/z 922.0097) as internal standards to ensure mass accuracy and reproducibility. Data were collected in a centroid mode and the mass range was set at m/z 50–1000 using extended dynamic range. Each sample was run in duplicate, and after data integration, the duplicate runs were averaged. Potential biomarkers were analyzed by MS/MS. MS spectra were collected at 2 spectra/s, and MS/MS spectra were collected at 0.5 spectra/s, with a medium isolation window (~4 *m/z*) and fixed collision energy of 15 V. A negative ion scan was only employed when metabolite identification was carried out.

Data Analysis

The GC-MS data and LC-MS data in an instrument-specific format were

converted to NetCDF and mzData formats via Thermo Xconvert software and Agilent MassHunter Qualitative software, respectively. The program XCMS was used for nonlinear alignment of the data in the time domain and automatic integration and extraction of the peak intensities. XCMS parameters were default settings except for the following: fwhm=4, bw=5 and snthersh=5 for GC-MS and fwhm=10, bw=10 and snthersh=5 for LC-MS. The variables presenting in at least 80% of either group were extracted [29]. Variables with less than 30% relative standard deviation (RSD) in QC samples [27] were then retained for further multivariate data analysis because they were considered stable enough for prolonged GC-MS or LC-MS analysis. The output data were imported into MATLAB 7.0 software (The MathWorks, Inc., USA), where the GC-MS data and LC-MS data of each sample were normalized to the sum of all peak areas of each sample and cell numbers. Then, data acquired from RP and HILIC columns were combined as a new dataset after the above pretreatment for multivariate statistical analysis. However, it should be noted that GC-MS data inherently contain apparent variability and complexity such as multiple fragment ions from a single compound. Directly concatenating the matrices of processed-MS data is suboptimal as this may result in a matrix with an unfavorable samples-to-variables ratio [30]. It is necessary to use properly reduced matrix to conduct multivariate statistical analysis. A simple strategy was untargeted filtration of ion peaks using our in-house scripts in the MATLAB 7.0, where the most abundant fragment ion with the same retention

time (the time bin is 0.01 min) was maintained and the other ions were excluded, as described in our previous report [20]. The remaining data list from GC-MS was further subjected to multivariate data analysis.

Multivariate data analysis based on the principal component analysis (PCA) and partial least-squares discriminant analysis (PLS-DA) was accomplished by using SIMCA-P V12.0.0 Demo (Umetrics, Sweden) after mean-centering and pareto-scaling, a technique that increases the importance of low abundance ions without significant amplification of noise. The quality of the models was evaluated with the relevant R^2 and Q^2 as well discussed elsewhere [31]. Statistically significant differences for the variables between the control, inaTat and Tat-treated groups were tested by ANOVA and the Tukey post hoc test for comparisons of multiple groups. The differences were considered significant when $p < 0.05$. To account for multiple comparisons, false discovery rate was estimated as the maximum q value [32] in the set of significant differences for the metabonomic data set. False discovery rates were computed using the R package q value (http://www.r-project.org/). The significance of the group differences was evaluated by the p value for the fixed-effect parameter estimate of group differences.

Identification of the metabolites based on GC–MS data was firstly performed by searching the NIST database installed in the Thermo-Finnigan Trace DSQ GC/MS system. Candidate compounds showing higher similarities (>75%) were then selected. Finally, the exact identities of the metabolites of

interest were verified by commercial standards.

Metabolite identification based on RPLC–MS and HILIC-MS data was carried out according to Tan et al [28]. Briefly, ions of interest were scanned in both negative and positive modes to facilitate the judgment of quasi-molecular ions. According to accurate mass, potential molecular formulae were calculated by Agilent MassHunter software. At the same time, structure information was obtained by searching freely accessible databases of HMDB (www.hmdb.ca), METLIN (http://metlin.scripps.edu) and KEGG (http://www.kegg.jp) utilizing detected molecular weights. Then, fragment ions were subjected to analysis through tandem MS to narrow the scope of target compounds. Finally, available commercial standards were adopted to validate the identification.

Metabolic Pathway Analysis

Metabolic pathway analysis was performed via MetaboAnalyst 2.0 (http://www.metaboanalyst.ca/MetaboAnalyst/) to identify the affected metabolic pathways analysis and visualization [33, 34].

Quantitative Real-Time PCR

RNA was isolated from 10^6 test and control cells using TRIzol reagent (Invitrogen, Carlsbad, CA) and then further purified utilizing the RNeasy mini kit (Qiagen, Chatsworth CA). cDNA was synthesized by using moloney murine

leukemia virus (M-MLV) reverse transcriptase (TaKaRa, Dalian, China) with random primers. Quantitative real-time PCR was performed using SYBR® Premix Ex Taq™ (Perfect Real Time) (TaKaRa, Dalian, China). Reactions were optimized and validated by dilutional analysis. Primer sequences were obtained from Eurogentec and are available in Supplemental Table 1. Reactions were performed in duplicate. To compute the relative amounts of target mRNA in the samples, the $2^{-\Delta\Delta CT}$ method was used [35]. Both glyceraldehyde-3-phosphate dehydrogenase (GAPDH) and β-actin were selected as internal controls. Changes in target gene expression in Tat and inaTat-treated cells, normalized to internal controls and relative to its expression in control cells, were calculated for each sample. The data $2^{-\Delta\Delta CT}$ obtained from qRT-PCR were subjected to ANOVA and difference was considered significant with $p < 0.05$.

Results

HIV-1 Tat Suppresses Proliferation of Jurkat Cells

To investigate the immunoregulatory effect of HIV-1 Tat, Jurkat cells (a $CD4^+$ T cell line often used in the study of interactions between Tat and T cells) [4, 36, 37], were used in this study. Briefly, 10^5 Jurkat T-cells were incubated with PBS, Tat or inaTat protein at a final concentration of 10 nM, 50 nM or 100 nM for 24 or 48 h. Inhibition on cell growth was calculated based on the absorbance at 570 nm. The result indicated that Tat had an obvious inhibitory

effect on cell proliferation at a high dose level. There was a significant difference in the level of proliferation between Tat and inaTat groups at 100 nM Tat at 24 and 48 h, when the inhibitory effect on lymphocyte proliferation was about 25% higher than that in inaTat group ($p < 0.05$) (Figure 2A), while there was no significant difference at 10 nM and 50 nM (data not shown).

HIV-1 Tat Induces Apoptosis of Jurkat cells

It is known that extracellular Tat protein induces apoptosis and increases sensitivity to apoptotic signals in both primary $CD4^+$ T-cells and T-cell lines, thus contributing in part to the progressive loss of T-cells associated with HIV-1 infection [3, 4]. Using FITC-annexin V staining of the cells, a significant difference in the level of apoptosis was observed at 100 nM Tat at 48 h, when apoptosis was about 10% greater than that in inaTat and control groups ($p < 0.05$) (Figures 2b and 2c), while no significant difference was observed at the other doses and time points.

Metabolic Profiling of GC-MS, RPLC-MS and HILIC-MS

The separation conditions of intra- and extra-cellular samples on three columns were optimized in terms of peak shape and reproducibility. To ensure repeatability of the analysis, the QC samples were processed as real samples and then were randomly inserted amongst the real sample queue to be analyzed eight times. Taking the results obtained from the intracellular samples

as an example, metabolic profile data pretreatment resulted in a final dataset consisting of 246, 692 and 891 metabolic features from GC-MS, RPLC-MS and HILIC-MS analyses, respectively. In GC-MS analysis, RSD (relative standard derivations) was less than 30% in more than 78% of the 246 metabolic features, which accounted for nearly 92% of the summed responses. The corresponding proportions were 85% and 94% for RPLC-MS and 87% and 95% for HILIC-MS analysis. Similar results were obtained from extracellular data. All the results indicated that the method was robust with good repeatability and stability.

Typical total ions current chromatograms (TICs) of the intra- and extra-cellular samples on GC, RPLC and HILIC are shown in Figure 3. The combination of RPLC, HILIC and GC chromatographic techniques could obviously add information about metabolites for the subsequent study. Here, several polar metabolites were only identified from HILIC-MS dataset, including L-carnitine, isobutyryl carnitine, propionyl-L-carnitine, sphingomyelin, *N*-methylnicotinamide and creatine. This result demonstrated that HILIC-MS analysis provided a different view of cellular composition, which could be a useful complementary tool to RPLC or GC analysis for metabolic profiling studies.

Multivariate Statistical Analyses and Identification of Intra- and Extra-cellular Metabolites

By untargeted filtration of ion peaks from GC-MS and integration of RPLC-MS and HILIC-MS, as described in Section “Data Analysis”, 246 ion peaks from intracellular GC-MS data and 1583 ion peaks from intracellular LC-MS data including 692 ions of RPLC-MS and 891 ions of HILIC-MS were obtained. Like intracellular metabonomic analysis, 286 ion peaks from extracellular GC-MS data and 973 ion peaks from extracellular LC-MS data including 469 ions of RPLC-MS and 504 ions of HILIC-MS were obtained. PCA was initially performed on the above GC-MS and LC-MS datasets to visualize general clustering trends among the observations, and a tendency in the score plot to separate Tat group from control and inaTat groups (Figure 4). This result suggested that Jurkat cells displayed distinct metabolic characteristics under Tat treatment, and inaTat protein caused changes similar to PBS control. To see whether the differentially expressed metabolites were accountable for the separation between Tat and inaTat groups, a more sophisticated PLS-DA was carried out on the GC-MS and LC-MS datasets. Tat group was clearly discriminated from inaTat and PBS groups by the primary component t (1) or the secondary component t (2) based on models with R^2X (cum) and R^2Y (cum) values of 0.70-0.88 and 0.82-0.92, respectively, indicating the goodness of fit of the data, and with Q^2 (cum) values of 0.73-0.83, estimating the predictive ability of the model (Table 1). In addition, the PLS-DA models were validated by a permutation test. *R* intercept values of all models, with the exception of the intracellular sample, analyzed by LC-MS were lower than 0.3 and their Q

intercept values were lower than -0.2, indicating that the models were not overfitted. Also, the *p*-values obtained from 7-fold cross validation [38, 39] showed that all groups fitted by different models were significantly different (Table 1).

To select potential biomarkers worthy of preferential study, metabolites that differed statistically significantly between the groups after correction for multiple comparisons (false discovery rate $q < 0.05$) were identified. Variables that significantly contributed to the clustering and discrimination were identified according to a threshold of variable importance in the projection (VIP) values (VIP > 1), which could be generated after PLS-DA processing. In addition, the criteria were further restricted to features with an average intensity difference of at least 1.5-fold (high or low) between inaTat- and Tat-induced samples. Significant peak changes between samples were confirmed by manual quantification by calculating the area under the peak from raw chromatograms. One of the significant metabolites eluted at 15.46 min on RPLC from intracellular samples was detected at *m/z* 302.306 $[M+H]^+$, its extracted ion chromatograms from intracellular samples of the control, inaTat and Tat treated Jurkat cells are given in Figure 3G. It can be observed that its level was significantly elevated in Tat-treated group comparing with control and inaTat groups.

Following the criterion above, 37 significantly changed metabolites were identified in both HIV-1 Tat-induced intracellular and extracellular metabolomes (Tables 2 and 3).

Metabolic Pathway Analysis

It is well-known that changes in more important positions of a network will trigger a more severe impact on the pathway than changes occurring in marginal or relatively isolated positions. Metabolic pathway analysis with MetaboAnalyst 2.0 revealed that identified differential metabolites are important for the cell response to Tat and are responsible for multiple pathways (Figure 5). The impact-value threshold calculated from pathway topology analysis was set to 0.10 [40], and 11 pathways among the regulated pathways were filtered out as potential targets pathway (Figure 5 and Table 4) for the Tat-treated cells, including sphingolipid metabolism, glycine, serine and threonine metabolism, pyruvate metabolism, inositol phosphate metabolism, arginine and proline metabolism, citrate cycle, phenylalanine metabolism, tryptophan metabolism, pentose phosphate pathway, glycerophospholipid metabolism, glycolysis or gluconeogenesis. By relating the metabolic pathways, the metabolic network of HIV Tat-induced potential biomarkers was constructed (Figure 6).

Quantitative RT-PCR Analysis for Key Enzymes Involved in the Pathways of Altered Metabolites

To validate the metabolic changes, the expression of key enzymes in these metabolic pathways was determined at gene levels using quantitative

real-time PCR analysis on cellular RNA from control, inaTat and Tat groups, including lactate dehydrogenase A (LDHA), succinate dehydrogenase (SDHB), malate dehydrogenase (MDH), serine palmitoyltransferase (SPT), acid sphingomyelinases (ASM), Phospholipase A1 member A (PLA1A), phospholipase A2 group IVC (PLA2G4C) and Indoleamine-2,3-dioxygenase (IDO). As shown in Figure 7, LDHA involved in glycolysis showed significant 2.5-fold upregulation. In citrate cycle, significant 3.4-fold downregulation of SDHB was observed, but there was no significant difference in MDH1 and MDH2 between Tat-treated and inaTat groups. In sphingolipid-related metabolic pathway, significant 3.1-fold upregulation of SPT1, 2.7-fold upregulation of SPT2, and 2.2-fold upregulation of ASM were observed. PLA1A and PLA2G4C involved in phospholipids metabolism showed 2.0-fold and 2.4-fold upregulation respectively. IDO (key enzyme of tryptophan metabolism) indicated 4.0-fold upregulation.

Discussion

Recent advances in metabonomic methodologies, such as LC–MS and GC-MS technologies, enable simultaneous measurement of numerous cellular metabolic intermediates, thus providing new insights into meaningful biological changes. Using these technologies, changes in metabonomic profiles have been clearly demonstrated in host cells where HIV and HCV replicate [16, 41]. Our previous study [20] observed HIV Tat protein-induced changes in

metabonomic profiles in mice. Knowing that HIV Tat protein possesses multiple biological activities and plays critical roles in HIV pathogenesis as a “viral toxin”, it has become an important target for drug intervention and therapeutic vaccines. Nevertheless, it is still necessary to further investigate its effects on cells at metabonomic levels.

The key issue in metabonomics is to exploit the information hidden in a complex metabolome. When it comes to analytical techniques, it is ideal that all metabolites, or as many metabolites as possible, can be detected within one assay. However, no technology available can fully fulfill the task, and therefore a combined integrative strategy is more common in the metabonomics field [42]. In this study, we simultaneously employed GC–MS and LC–MS techniques based on the consideration of balancing the detection of volatile and non-volatile components, as well as HILIC-MS and RPLC-MS based on the consideration of balancing the detection of polar and non-polar or medium polar components. It was demonstrated that the parallel use of RPLC-MS, HILIC-MS and GC-MS could acquire more metabolite information and gain deeper insights into biological mechanisms.

Metabolite secretion by a cell reflects the biochemical response to external stimuli. For complete analysis of a cell culture, it is important to measure both extracellular (footprint) and intracellular (fingerprint) metabolic profiles [43]. Simultaneous measurement of extracellular and intracellular metabolic profiles provided us a confirmatory or complementary understanding about the overall

cellular response. To obtain the information about metabolic variations underlying the treatment of Tat, we simultaneously analysed the intracellular and extracellular metabolome in Jurkat cells. Thirty-seven metabolites related with Tat treatment were identified with statistically significant changes.

To identify the most relevant metabolic pathways involved in metabolic reprogramming of Tat-treated Jurkat cells, the differential metabolites were further subjected to MetaboAnalyst 2.0. The eleven most relevant pathways of Tat-treated Jurkat cell were identified. Based on our findings, an integrative view plot of the metabolic changes induced by Tat protein in Jurkat cells is shown in Figure 6, which involved in 37 differential metabolites and 10 relevant key enzymes as well as 11 major perturbed metabolic pathways. The major perturbed metabolic patterns and plausible pathways in Tat-treated Jurkat cells are discussed below.

Sphingomyelin (SM), sphinganine, sphingosine and ceramide are classified as sphingolipids, and play important roles in the sphingolipids biosynthesis and metabolism. Sphingolipids have been regarded as important signal molecules that mediate many biological functions such as cell growth, differentiation, senescence and apoptosis [44, 45]. It was found in our study that SM was decreased, and sphinganine, sphingosine and ceramide were increased markedly in Tat-treated cells. Understandably, these metabolic disorders could originate from the regulation of some key enzymes associated with sphingolipid metabolism. It is known that sphingomyelinases (SMases)

hydrolyse SM, releasing ceramide and creating a cascade of bioactive lipids such as sphinganine and sphingosine [46]. Real-time PCR in this study showed that acid SMases (ASM) were found to be upregulated in Tat-treated group, which have been repeatedly implicated as effectors in pro-apoptotic pathways [47]. In addition, two subunits SPT1 and SPT2 of serine palmitoyltransferas (SPT), the rate-limiting enzyme of de-novo synthesis of ceramide, were also upregulated, which probably contributed to the accumulation of ceramides in cells. This finding is consistent with a previous report indicating that SPT1 gene was significantly upregulated in Tat-induced cells [48]. High levels of sphingosine and/or ceramide can inhibit cell proliferation and migration and promote apoptosis [44], which could correlate with the inhibition of cell proliferation and induction of apoptosis in uninfected lymphocytes by HIV-1 Tat protein as reported in previous studies [4, 36] and were also confirmed in our study (see Figure 2).

LPC, as endogenous phospholipids, is very important and can mediate many cell signaling pathways in macrophages and T cells [49, 50] and specific receptors [51], so that it participates in inflammatory response. Increased LPC and decreased PC in Tat-treated group indicated a disturbance of glycerophospholipid catabolism. It is conceivable that these alterations may ascribe to the activation of phospholipase A2. Indeed, it was found in Tat-treated group that 2 phospholipases were increased. PLA1A is a secreted enzyme that hydrolyzes phosphatidylserine and

1-acyl-2-lysophosphatidylserine to produce 2-acyl-1-lysophosphatidylserine, glycerophosphoserines, and free fatty acids [52]. PLA2G4C is a membrane-associated enzyme that sequentially hydrolyzes fatty acid from the sn-2 and sn-1 positions of PC, releasing LPC in addition to saturated and unsaturated fatty acids. In contrast to the well-characterized PLA2A, PLA2G4C does not show specificity for arachidonic acid and can release large amounts of oleic and palmitic acids [53], both of which were found to be increased in Tat-treated group. It was reported that LPC could up-regulate CXCR4 chemokine receptor expression in human $CD4^+$ T cells that is critical for infection by X4 HIV-1 strains [54], indicating that LPC played a potentially important role in rendering bystander $CD4^+$ T cells to be more susceptible to HIV-1 infection as induced by extracellular Tat.

Lactate, glucose and G-3-P were correlated with glycolysis, indicating the modulation of the glycolytic pathway. An elevation in lactate level was observed in Tat-treated group. It is conceivable that the reduction should be accompanied with upregulation of lactate dehydrogenase (LDH) which could result in lactate increase through the conversion of pyruvate to lactate. This hypothesis was verified by quantitative real-time PCR, which revealed significant upregulation of LDHA in Tat-treated cells. The build-up of G-3-P was also observed in Tat-treated group, which is consistent with the result of Hollenbaugh *et al* [16]. These data, together with the increased lactate level, suggest an increased rate of glycolysis for HIV Tat-induced $CD4^+$ T cells.

Additionally, glucose was also found to be elevated in Tat-treated group. It is known that HIV-infected patients have an increased prevalence of impaired glucose tolerance and diabetes mellitus [28]. It was also reported that Tat could induce TNF-α production, block FFA uptake by adipocytes and suppress insulin receptor signaling, all of which could potentially decrease glucose disposal [55, 56]. These reports are in agreement with our result that glucose was increased in Tat-treated T cells.

The citrate cycle is central to aerobic metabolism, facilitating adequate throughout of substrates derived from carbohydrates, fatty acids or certain amino acids. Changes in three pivotal intermediates of citrate cycle were observed in this study, where the low level of citrate and high level of succinate and malate were observed in Tat-treated group. It could be presumed that a decreased utilization of glucose as the substrate could, at least in part, lead to the reduction of citrate synthesis. However, the elevation of succinate and malate could result from the regulation of some key enzymes associated with the citrate cycle. It is known that the metabolism of succinate and malate depends on succinate dehydrogenase (SDH) and malate dehydrogenase (MDH). Real-time PCR showed that SDHB was downregulated in Tat-treated group, which probably contributed to the elevation of succinate, but MDH showed no significant difference between the three groups. We speculate that the elevation of malate may be caused by other factors.

Carnitine was remarkably reduced in Tat-treated cells. Because of the key

role that carnitine plays in synthesis and *β*-oxidation of fatty acid, there may be some problems in the mitochondrial metabolism in Tat-treated group. Several previous studies [57, 58] indicated that carnitine supplements reduced the frequency of apoptotic CD4 and CD8 cells and the level of ceramide in HIV-infected individuals, which provides indirect evidence for its reduction. Di Marzio L [59] reported that L-carnitine inhibited the apoptosis and ceramide production of both HuT78 and U937 cell lines, which appears to be related to the inhibition of an acidic sphingomyelinase. In this study, Tat-induced reduction in carnitine and increase in apoptosis were both observed in Jurkat cell line (Figure 2B and 2C), which provides metabolic evidence to support the idea that carnitine supplements may be an attractive approach for the treatment of apoptosis of $CD4^+$ T cells.

The low levels of valine and isoleucine, two branched-chain amino acids (BCAAs), were observed in Tat-treated group. BCAAs may be an important alternative energy substrate. It seems that the reduction in ATP production due to the inhibition of citrate cycle induced by Tat as discussed above could lead to the utilization of BCAAs as energy compensation. LC-MS and GC-MS spectra also showed changes in the metabolism of other α-amino acids, as represented by increased levels of L-alanine, glycine, and proline in Tat-treated group. α-amino acids are important energy metabolism precursors and can be transformed into some biomolecules, such as pyruvate, 2-oxoglutarate and fumarate, to enter the citrate cycle. One possible

speculation is that Tat leads to metabolic remodeling of α-amino acids to meet the energy requirement in Jurkat cells. In addition, the alterations in energy metabolism induced by Tat were associated with ATP depletion and accumulation of phosphate.

Metabolism of phenylalanine was found to be associated with HIV-1 pathology: higher phenylalanine/tyrosine (phe/tyr) shows an association with lower $CD4^+$ cell counts and with higher HIV-RNA levels. Even stronger associations exist between phe/tyr and phe and tyr concentrations and concentrations of immune activation marker neopterin in urine and plasma [60]. In our study, the increase of phe and decrease of tyr were found in Tat-treated group, which probably contribute to the loss and immune activation of Jurkat cell.

Decreased tryptophan and increased N-methylnicotinamide were detected in Tat-treated group, indicating that tryptophan metabolism was elevated. Real-time PCR showed that IDO, the rate-limiting enzyme of tryptophan metabolism, was upregulated, which is consistent with the study of Samikkannu et al [61], who indicated that tryptophan was degraded as Tat up-regulated IDO in immature dendritic cells. Tryptophan catabolism mediated by IDO is an immunoregulatory mechanism that limits T-cell proliferation by depletion of the essential amino acid tryptophan and/or accumulation of catabolites with immune-suppressive activity [62]. This Tat-induced abnormal tryptophan metabolism in Jurkat cells could be associated with its

immunosuppression, as validated by MTT assays in this study. It should be noted that the study with the RP mode cannot detect the metabolite of tryptophan, perhaps, in that it had a relatively high polar and was unretained on RP column. Finally, changes in cholesterol and myo-inositol levels were also observed in Tat-treated group, which was perplexing due to a lack of information about their biology pathways.

In conclusion, this is the first metabonomic study to determine intra- and extra-cellular biochemical alterations of HIV-1 Tat-treated Jurkat cells by using combined LC-MS and GC-MS. We have identified 37 significantly changed metabolites and predicted the major metabolites network of Tat-treated Jurkat cells by pattern recognition and pathway analysis. Combining the results from these methods, we have calculated 11 high confidence networks (Impact score>0.10). The identified target metabolites were found to encompass a variety of pathways related to sphingolipid metabolism, glycine, serine and threonine metabolism, pyruvate metabolism, inositol phosphate metabolism, arginine and proline metabolism, citrate cycle, phenylalanine metabolism, tryptophan metabolism, pentose phosphate pathway, glycerophospholipid metabolism, glycolysis or gluconeogenesis, which were helpful for revealing the complex pathogenic mechanism of HIV-1 Tat as a “viral toxin” and may present important targets for therapeutic intervention. Blocking or modifying these points of convergence and HIV protein-induced apoptotic pathways are attractive approaches to the treatment of depletion of $CD4^+$ T cells caused by

HIV infection. Further studies are needed to deepen the understanding about the biological function and regulation mechanism of HIV-1 Tat protein. In addition, our findings suggest that metabonomics based on integration of GC-MS and LC-MS techniques could be a potent tool for cell metabolomes.

Acknowledgements

This work was funded by the National Natural Science Foundation of China (NSFC) [Grant numbers 30972632 and 30872405], Shanghai Committee of Science and Technology [08JC1405200], the Chinese National Key Special Project for the Prevention and Control of Major Infectious Diseases [2009ZX10004-105], and the Chinese National Key Special Project for Major New Drug Discovery [2011ZX09506-001].

Supporting Information

Supplementary table. This material is available free of charge via the Internet at http://pubs.acs.org.

References

1. Fauci, A. S., Host factors and the pathogenesis of HIV-induced disease. *Nature* **1996,** 384, (6609), 529-34.

2. Li, J. C.; Yim, H. C.; Lau, A. S., Role of HIV-1 Tat in AIDS pathogenesis: its effects on cytokine dysregulation and contributions to the pathogenesis of

opportunistic infection. *Aids* **2010,** 24, (11), 1609-23.

3. Westendorp, M. O.; Frank, R.; Ochsenbauer, C.; Stricker, K.; Dhein, J.; Walczak, H.; Debatin, K. M.; Krammer, P. H., Sensitization of T cells to CD95-mediated apoptosis by HIV-1 Tat and gp120. *Nature* **1995,** 375, (6531), 497-500.

4. Li, C. J.; Friedman, D. J.; Wang, C.; Metelev, V.; Pardee, A. B., Induction of apoptosis in uninfected lymphocytes by HIV-1 Tat protein. *Science* **1995,** 268, (5209), 429-31.

5. Secchiero, P.; Zella, D.; Capitani, S.; Gallo, R. C.; Zauli, G., Extracellular HIV-1 tat protein up-regulates the expression of surface CXC-chemokine receptor 4 in resting CD4+ T cells. *J Immunol* **1999,** 162, (4), 2427-31.

6. Campbell, G. R.; Loret, E. P.; Spector, S. A., HIV-1 Clade B Tat, but Not Clade C Tat, Increases X4 HIV-1 Entry into Resting but Not Activated CD4(+) T Cells. *Journal of Biological Chemistry* **2010,** 285, (3), 1681-1691.

7. Gallo, R. C., Tat as one key to HIV-induced immune pathogenesis and Pat toroid as an important component of a vaccine. *Proceedings of the National Academy of Sciences of the United States of America* **1999,** 96, (15), 8324-8326.

8. Longo, O.; Tripiciano, A.; Fiorelli, V.; Bellino, S.; Scoglio, A.; Collacchi, B.; Alvarez, M. J.; Francavilla, V.; Arancio, A.; Paniccia, G.; Lazzarin, A.; Tambussi, G.; Din, C. T.; Visintini, R.; Narciso, P.; Antinori, A.; D'Offizi, G.; Giulianelli, M.; Carta, M.; Di Carlo, A.; Palamara, G.; Giuliani, M.; Laguardia, M. E.; Monini, P.;

Magnani, M.; Ensoli, F.; Ensoli, B., Phase I therapeutic trial of the HIV-1 Tat protein and long term follow-up. *Vaccine* **2009,** 27, (25-26), 3306-12.

9. Ensoli, B.; Bellino, S.; Tripiciano, A.; Longo, O.; Francavilla, V.; Marcotullio, S.; Cafaro, A.; Picconi, O.; Paniccia, G.; Scoglio, A.; Arancio, A.; Ariola, C.; Ruiz Alvarez, M. J.; Campagna, M.; Scaramuzzi, D.; Iori, C.; Esposito, R.; Mussini, C.; Ghinelli, F.; Sighinolfi, L.; Palamara, G.; Latini, A.; Angarano, G.; Ladisa, N.; Soscia, F.; Mercurio, V. S.; Lazzarin, A.; Tambussi, G.; Visintini, R.; Mazzotta, F.; Di Pietro, M.; Galli, M.; Rusconi, S.; Carosi, G.; Torti, C.; Di Perri, G.; Bonora, S.; Ensoli, F.; Garaci, E., Therapeutic immunization with HIV-1 Tat reduces immune activation and loss of regulatory T-cells and improves immune function in subjects on HAART. *PLoS One* **2010,** 5, (11), e13540.

10. Nazih, H.; Raffi, F.; Taieb, A.; Reynes, J.; Choutet, P.; Cassuto, J. P.; Ferry, T.; Chene, G.; Leport, C.; Bard For The Aproco-Copilote Anrs Co 08 Study Group, J. M., Peroxisome Proliferator Activating Receptor (PPAR) Alpha and Gamma Polymorphisms and Metabolic Abnormalities in HIV-Infected Patients Receiving Highly Active Antiretroviral Therapy: The ANRS CO8 APROCO-COPILOTE Study. *AIDS Res Hum Retroviruses* **2011**.

11. Bevilacqua, M.; Dominguez, L. J.; Barbagallo, M., Insulin Resistance and the cardiometabolic syndrome in HIV infection. *J Cardiometab Syndr* **2009,** 4, (1), 40-3.

12. Grima, P.; Guido, M.; Chiavaroli, R.; Stano, F.; Tundo, P.; Tana, M.; de Donno, A.; Zizza, A., Altered phosphate metabolism in HIV-1-infected patients

with metabolic syndrome. *Scand J Infect Dis* **2011**.

13. Gutierrez, A. D.; Balasubramanyam, A., Dysregulation of glucose metabolism in HIV patients: epidemiology, mechanisms, and management. *Endocrine* **2011**.

14. Fiehn, O., Metabolomics--the link between genotypes and phenotypes. *Plant Mol Biol* **2002,** 48, (1-2), 155-71.

15. Munger, J.; Bennett, B. D.; Parikh, A.; Feng, X. J.; McArdle, J.; Rabitz, H. A.; Shenk, T.; Rabinowitz, J. D., Systems-level metabolic flux profiling identifies fatty acid synthesis as a target for antiviral therapy. *Nat Biotechnol* **2008,** 26, (10), 1179-86.

16. Hollenbaugh, J. A.; Munger, J.; Kim, B., Metabolite profiles of human immunodeficiency virus infected CD4+ T cells and macrophages using LC-MS/MS analysis. *Virology* **2011**.

17. Ruiz-Aracama, A.; Peijnenburg, A.; Kleinjans, J.; Jennen, D.; van Delft, J.; Hellfrisch, C.; Lommen, A., An untargeted multi-technique metabolomics approach to studying intracellular metabolites of HepG2 cells exposed to 2,3,7,8-tetrachlorodibenzo-p-dioxin. *BMC Genomics* **2011,** 12, 251.

18. Lin, L.; Huang, Z.; Gao, Y.; Yan, X.; Xing, J.; Hang, W., LC-MS based serum metabonomic analysis for renal cell carcinoma diagnosis, staging, and biomarker discovery. *J Proteome Res* **2011,** 10, (3), 1396-405.

19. Wu, Z.; Li, M.; Zhao, C.; Zhou, J.; Chang, Y.; Li, X.; Gao, P.; Lu, X.; Li, Y.; Xu, G., Urinary metabonomics study in a rat model in response to

protein-energy malnutrition by using gas chromatography-mass spectrometry and liquid chromatography-mass spectrometry. *Mol Biosyst* **2010,** 6, (11), 2157-63.

20. Liao, W.; Tan, G.; Zhu, Z.; Chen, Q.; Lou, Z.; Dong, X.; Zhang, W.; Pan, W.; Chai, Y., HIV-1 Tat induces biochemical changes in the serum of mice. *Virology* **2012,** 422, (2), 288-96.

21. Ensoli, B.; Buonaguro, L.; Barillari, G.; Fiorelli, V.; Gendelman, R.; Morgan, R. A.; Wingfield, P.; Gallo, R. C., Release, uptake, and effects of extracellular human immunodeficiency virus type 1 Tat protein on cell growth and viral transactivation. *J Virol* **1993,** 67, (1), 277-87.

22. Avraham, H. K.; Jiang, S.; Lee, T. H.; Prakash, O.; Avraham, S., HIV-1 Tat-mediated effects on focal adhesion assembly and permeability in brain microvascular endothelial cells. *J Immunol* **2004,** 173, (10), 6228-33.

23. Perry, S. W.; Barbieri, J.; Tong, N.; Polesskaya, O.; Pudasaini, S.; Stout, A.; Lu, R.; Kiebala, M.; Maggirwar, S. B.; Gelbard, H. A., Human immunodeficiency virus-1 Tat activates calpain proteases via the ryanodine receptor to enhance surface dopamine transporter levels and increase transporter-specific uptake and Vmax. *J Neurosci* **2010,** 30, (42), 14153-64.

24. Chi, X.; Amet, T.; Byrd, D.; Chang, K.-H.; Shah, K.; Hu, N.; Grantham, A.; Hu, S.; Duan, J.; Tao, F.; Nicol, G.; Yu, Q., Direct Effects of HIV-1 Tat on Excitability and Survival of Primary Dorsal Root Ganglion Neurons: Possible Contribution to HIV-1-Associated Pain. *PLoS ONE* **2011,** 6, (9), e24412.

25. Himer, L.; Csoka, B.; Selmeczy, Z.; Koscso, B.; Pocza, T.; Pacher, P.; Nemeth, Z. H.; Deitch, E. A.; Vizi, E. S.; Cronstein, B. N.; Hasko, G., Adenosine A2A receptor activation protects CD4+ T lymphocytes against activation-induced cell death. *Faseb J* **2010,** 24, (8), 2631-40.

26. Dietmair, S.; Timmins, N. E.; Gray, P. P.; Nielsen, L. K.; Kromer, J. O., Towards quantitative metabolomics of mammalian cells: development of a metabolite extraction protocol. *Anal Biochem* **2010,** 404, (2), 155-64.

27. Sangster, T.; Major, H.; Plumb, R.; Wilson, A. J.; Wilson, I. D., A pragmatic and readily implemented quality control strategy for HPLC-MS and GC-MS-based metabonomic analysis. *Analyst* **2006,** 131, (10), 1075-8.

28. Tan, G.; Lou, Z.; Liao, W.; Dong, X.; Zhu, Z.; Li, W.; Chai, Y., Hydrophilic interaction and reversed-phase ultraperformance liquid chromatography TOF-MS for serum metabonomic analysis of myocardial infarction in rats and its applications. *Mol Biosyst* **2011**.

29. Bijlsma, S.; Bobeldijk, I.; Verheij, E. R.; Ramaker, R.; Kochhar, S.; Macdonald, I. A.; van Ommen, B.; Smilde, A. K., Large-scale human metabolomics studies: a strategy for data (pre-) processing and validation. *Anal Chem* **2006,** 78, (2), 567-74.

30. Smilde, A. K.; van der Werf, M. J.; Bijlsma, S.; van der Werff-van der Vat, B. J.; Jellema, R. H., Fusion of mass spectrometry-based metabolomics data. *Anal Chem* **2005,** 77, (20), 6729-36.

31. Yin, P.; Wan, D.; Zhao, C.; Chen, J.; Zhao, X.; Wang, W.; Lu, X.; Yang, S.;

Gu, J.; Xu, G., A metabonomic study of hepatitis B-induced liver cirrhosis and hepatocellular carcinoma by using RP-LC and HILIC coupled with mass spectrometry. *Mol Biosyst* **2009,** 5, (8), 868-76.

32. Storey, J. D., A direct approach to false discovery rates. *J Royal Statistic Soc Ser B* **2002,** 64, 479-498.

33. Xia, J.; Mandal, R.; Sinelnikov, I. V.; Broadhurst, D.; Wishart, D. S., MetaboAnalyst 2.0--a comprehensive server for metabolomic data analysis. *Nucleic Acids Res* **2012,** 40, (W1), W127-W133.

34. Xia, J.; Wishart, D. S., Web-based inference of biological patterns, functions and pathways from metabolomic data using MetaboAnalyst. *Nat Protoc* **2011,** 6, (6), 743-60.

35. Livak, K. J.; Schmittgen, T. D., Analysis of relative gene expression data using real-time quantitative PCR and the 2(-Delta Delta C(T)) Method. *Methods* **2001,** 25, (4), 402-8.

36. Campbell, G. R.; Pasquier, E.; Watkins, J.; Bourgarel-Rey, V.; Peyrot, V.; Esquieu, D.; Barbier, P.; de Mareuil, J.; Braguer, D.; Kaleebu, P.; Yirrell, D. L.; Loret, E. P., The glutamine-rich region of the HIV-1 Tat protein is involved in T-cell apoptosis. *J Biol Chem* **2004,** 279, (46), 48197-204.

37. Coiras, M.; Camafeita, E.; Urena, T.; Lopez, J. A.; Caballero, F.; Fernandez, B.; Lopez-Huertas, M. R.; Perez-Olmeda, M.; Alcami, J., Modifications in the human T cell proteome induced by intracellular HIV-1 Tat protein expression. *Proteomics* **2006,** 6 Suppl 1, S63-73.

38. Mahadevan, S.; Shah, S. L.; Marrie, T. J.; Slupsky, C. M., Analysis of metabolomic data using support vector machines. *Analytical Chemistry* **2008,** 80, (19), 7562-7570.

39. Pasikanti, K. K.; Esuvaranathan, K.; Ho, P. C.; Mahendran, R.; Kamaraj, R.; Wu, Q. H.; Chiong, E.; Chan, E. C. Y., Noninvasive Urinary Metabonomic Diagnosis of Human Bladder Cancer. *Journal of Proteome Research* **2010,** 9, (6), 2988-2995.

40. Wang, X.; Yang, B.; Sun, H.; Zhang, A., Pattern recognition approaches and computational systems tools for ultra performance liquid chromatography-mass spectrometry-based comprehensive metabolomic profiling and pathways analysis of biological data sets. *Anal Chem* **2012,** 84, (1), 428-39.

41. Roe, B.; Kensicki, E.; Mohney, R.; Hall, W. W., Metabolomic profile of hepatitis C virus-infected hepatocytes. *PLoS One* **2011,** 6, (8), e23641.

42. van der Werf, M. J.; Jellema, R. H.; Hankemeier, T., Microbial metabolomics: replacing trial-and-error by the unbiased selection and ranking of targets. *J Ind Microbiol Biotechnol* **2005,** 32, (6), 234-52.

43. Cuperlovic-Culf, M.; Barnett, D. A.; Culf, A. S.; Chute, I., Cell culture metabolomics: applications and future directions. *Drug Discov Today* **2010,** 15, (15-16), 610-21.

44. Yopp, A. C.; Randolph, G. J.; Bromberg, J. S., Leukotrienes, sphingolipids, and leukocyte trafficking. *J Immunol* **2003,** 171, (1), 5-10.

45. Olivera, A.; Rivera, J., Sphingolipids and the balancing of immune cell function: lessons from the mast cell. *J Immunol* **2005,** 174, (3), 1153-8.

46. Pavoine, C.; Pecker, F., Sphingomyelinases: their regulation and roles in cardiovascular pathophysiology. *Cardiovasc Res* **2009,** 82, (2), 175-83.

47. Steinbrecher, U. P.; Gomez-Munoz, A.; Duronio, V., Acid sphingomyelinase in macrophage apoptosis. *Curr Opin Lipidol* **2004,** 15, (5), 531-7.

48. Liang WS, M. A., Teslovich TM, de la Fuente C, Agbottah E, Dadgar S, Kehn K, Hautaniemi S, Pumfery A, Stephan DA, Kashanchi F., Therapeutic targets for HIV-1 infection in the host proteome. *Retrovirology. .* **2005,** Mar 21;2:20.

49. Duong, C. Q.; Bared, S. M.; Abu-Khader, A.; Buechler, C.; Schmitz, A.; Schmitz, G., Expression of the lysophospholipid receptor family and investigation of lysophospholipid-mediated responses in human macrophages. *Biochim Biophys Acta* **2004,** 1682, (1-3), 112-9.

50. Kabarowski, J. H., G2A and LPC: regulatory functions in immunity. *Prostaglandins Other Lipid Mediat* **2009,** 89, (3-4), 73-81.

51. Oestvang, J.; Johansen, B., PhospholipaseA2: a key regulator of inflammatory signalling and a connector to fibrosis development in atherosclerosis. *Biochim Biophys Acta* **2006,** 1761, (11), 1309-16.

52. Aoki, J.; Nagai, Y.; Hosono, H.; Inoue, K.; Arai, H., Structure and function of phosphatidylserine-specific phospholipase A1. *Biochim Biophys Acta* **2002,** 1582, (1-3), 26-32.

53. Stewart, A.; Ghosh, M.; Spencer, D. M.; Leslie, C. C., Enzymatic properties of human cytosolic phospholipase A(2)gamma. *J Biol Chem* **2002,** 277, (33), 29526-36.

54. Han, K. H.; Hong, K. H.; Ko, J.; Rhee, K. S.; Hong, M. K.; Kim, J. J.; Kim, Y. H.; Park, S. J., Lysophosphatidylcholine up-regulates CXCR4 chemokine receptor expression in human CD4 T cells. *J Leukoc Biol* **2004,** 76, (1), 195-202.

55. Kino, T.; Mirani, M.; Alesci, S.; Chrousos, G. P., AIDS-related lipodystrophy/insulin resistance syndrome. *Horm Metab Res* **2003,** 35, (3), 129-36.

56. Brown, T. T.; Tassiopoulos, K.; Bosch, R. J.; Shikuma, C.; McComsey, G. A., Association between systemic inflammation and incident diabetes in HIV-infected patients after initiation of antiretroviral therapy. *Diabetes Care* **2010,** 33, (10), 2244-9.

57. Cifone, M. G.; Alesse, E.; Di Marzio, L.; Ruggeri, B.; Zazzeroni, F.; Moretti, S.; Famularo, G.; Steinberg, S. M.; Vullo, E.; De Simone, C., Effect of L-carnitine treatment in vivo on apoptosis and ceramide generation in peripheral blood lymphocytes from AIDS patients. *Proc Assoc Am Physicians* **1997,** 109, (2), 146-53.

58. Moretti, S.; Alesse, E.; Di Marzio, L.; Zazzeroni, F.; Ruggeri, B.; Marcellini, S.; Famularo, G.; Steinberg, S. M.; Boschini, A.; Cifone, M. G.; De Simone, C., Effect of L-carnitine on human immunodeficiency virus-1 infection-associated

apoptosis: a pilot study. *Blood* **1998,** 91, (10), 3817-24.

59. Di Marzio, L.; Alesse, E.; Roncaioli, P.; Muzi, P.; Moretti, S.; Marcellini, S.; Amicosante, G.; De Simone, C.; Cifone, M. G., Influence of L-carnitine on CD95 cross-lining-induced apoptosis and ceramide generation in human cell lines: correlation with its effects on purified acidic and neutral sphingomyelinases in vitro. *Proc Assoc Am Physicians* **1997,** 109, (2), 154-63.

60. Zangerle, R.; Kurz, K.; Neurauter, G.; Kitchen, M.; Sarcletti, M.; Fuchs, D., Increased blood phenylalanine to tyrosine ratio in HIV-1 infection and correction following effective antiretroviral therapy. *Brain Behav Immun* **2010,** 24, (3), 403-8.

61. Samikkannu, T.; Rao, K. V.; Gandhi, N.; Saxena, S. K.; Nair, M. P., Human immunodeficiency virus type 1 clade B and C Tat differentially induce indoleamine 2,3-dioxygenase and serotonin in immature dendritic cells: Implications for neuroAIDS. *J Neurovirol* **2010,** 16, (4), 255-63.

62. Boasso, A.; Herbeuval, J. P.; Hardy, A. W.; Anderson, S. A.; Dolan, M. J.; Fuchs, D.; Shearer, G. M., HIV inhibits CD4+ T-cell proliferation by inducing indoleamine 2,3-dioxygenase in plasmacytoid dendritic cells. *Blood* **2007,** 109, (8), 3351-9.

Table 1. Summary of Parameters for Assessment of the Quality of PCA and PLS-DA Models

		models	no.[a]	R^2X_{cum}[b]	R^2Y_{cum}[b]	Q^2Y_{cum}[b]	R intercept[c]	Q intercept[c]	*p*[d]
intracellular	GC-MS	PCA	2	0.711	-	0.402	-	-	-
		PLS-DA	4	0.877	0.898	0.730	0.256	-0.533	0.029
	LC-MS	PCA	2	0.691	-	0.487	-	-	-
		PLS-DA	4	0.818	0.920	0.682	0.540	-0.396	0.043
extracellular	GC-MS	PCA	2	0.773	-	0.396	-	-	-
		PLS-DA	2	0.768	0.817	0.753	0.223	-0.216	0.013
	LC-MS	PCA	2	0.695	-	0.555	-	-	-
		PLS-DA	2	0.694	0.883	0.825	0.216	-0.299	0.000

[a] No. is the number of components. [b] R^2X_{cum} and R^2Y_{cum} are the cumulative modeled variation in X and Y matrix, respectively, and Q^2Y_{cum} is the cumulative predicted variation in Y matrix. [c] R and Q were obtained after permutation test (n = 999). [d] *P is p* value obtained from cross validation ANOVA of PLS-DA.

Table 2. Identification of differentiating metabolic features detected by using GC-MS and their metabolic pathways

no.	tr/min	metabolites identified	MS fragments	trend[a]	fold change[b]	related pathway	%RSD[d]	p(ANOVA)	q(ANOVA)	p(Tat/inaTat)
intracellular										
1	9.08	Lactate	191,147, 117, 73	↑	1.5	Glycolysis	12.1	1.36E-05	3.35E-04	3.95E-04
2	10.36	L-Alanine	147, 116, 73	↑	1.8	Amino acid metabolism	4.3	2.88E-05	5.90E-04	1.40E-04
3	12.55	Valine	218, 144, 73	↓	0.5	BCAA[c] metabolism	5.4	3.57E-05	6.57E-04	2.70E-05
4	16.28	Phosphate	314, 299, 73	↑	1.6	Energy metabolism	7.5	6.20E-04	1.70E-03	9.13E-04
5	16.73	Isoleucine	188, 147, 86, 75	↓	0.6	BCAA metabolism	6.8	2.00E-04	8.98E-04	8.56E-04
6	17.03	Glycine	248, 174, 147, 73	↑	1.6	Amino acid metabolism	3.7	4.20E-06	1.72E-04	6.04E-06
7	17.81	Succinate	247, 147, 73	↑	2.3	Citrate cycle	4.9	5.08E-04	1.42E-03	7.83E-04
8	22.55	Malate	233, 147, 73	↑	2.5	Citrate cycle	7.4	2.64E-07	2.16E-05	1.95E-06
9	24.28	Proline	230, 156, 73	↑	1.6	Proline metabolism	5.8	2.51E-05	5.61E-04	8.65E-05
10	26.96	Phenylalanine	218, 192, 147, 73	↑	3.0	Phenylalanine metabolism	10.3	8.45E-06	2.51E-04	1.53E-05
11	30.20	G-3-P	357, 299, 147, 73	↑	2.4	Glycolysis	9.0	2.28E-04	9.51E-04	7.67E-04
12	31.26	Glucose	319, 205, 147, 73	↑	2.4	Carbohydrate Metabolism	11.7	8.78E-07	5.40E-05	1.39E-06
13	35.15	Myo-Inositol	305, 217, 147, 73	↑	2.6	Inositol phosphate metabolism	6.9	1.06E-09	2.61E-07	4.21E-09
14	37.70	Palmitic acid	313, 117, 73	↑	2.6	Fatty acid metabolism	8.3	5.83E-06	2.05E-04	2.36E-05
15	41.76	Oleic acid	315, 129, 93, 73	↑	2.2	Fatty acid metabolism	5.6	9.20E-06	2.51E-04	4.19E-05
16	41.63	Stearic acid	341, 117, 73	↑	1.7	Fatty acid metabolism	6.4	1.38E-04	6.57E-04	1.51E-03
17	49.78	Cholesterol	458, 329, 129, 73	↑	2.2	Fatty acid metabolism	8.9	1.52E-07	1.87E-05	4.42E-07
extracellular										
1	9.06	Lactate	191,147, 117, 73	↑	1.5	Glycolysis	10.2	1.48E-07	1.41E-05	3.19E-07
2	10.32	L-Alanine	147, 116, 73	↑	1.8	Amino acid metabolism	3.5	3.64E-07	2.60E-05	5.31E-07
3	16.22	Phosphate	314, 299, 73	↑	1.8	Energy metabolism	6.3	7.02E-07	3.79E-05	1.58E-06
4	16.75	Isoleucine	188, 147, 86, 75	↓	0.6	BCAA[c]metabolism	5.4	1.05E-06	3.79E-05	4.51E-05
5	18.18	Propanoic acid	292, 189, 147, 73	↑	1.5	Fatty acid metabolism	11.1	4.40E-04	1.49E-03	2.39E-03
6	22.59	Malate	233, 147, 73	↑	1.6	Citrate cycle	6.5	1.02E-07	1.41E-05	1.49E-07

7	24.22	Proline	230, 156, 73	↑	3.6	Proline metabolism	4.3	8.98E-10	2.57E-07	2.48E-09
8	26.92	Phenylalanine	218, 192, 147, 73	↑	1.6	Phenylalanine metabolism	9.3	8.99E-07	3.79E-05	4.06E-06
9	32.60	Citrate	363, 273, 147, 73	↓	0.7	Citrate cycle	4.7	1.06E-06	3.79E-05	8.66E-06
10	33.73	Tyrosine	280, 218, 73	↓	0.6	Tyrosine metabolism	5.5	3.69E-06	1.17E-04	2.64E-05
11	37.75	Palmitic acid	313, 117, 73	↑	1.9	Fatty acid metabolism	3.7	6.44E-06	1.84E-04	1.07E-05
12	41.65	Stearic acid	341, 117, 73	↑	1.8	Fatty acid metabolism	5.8	5.36E-05	6.79E-04	8.21E-05
13	49.73	Cholesterol	458, 329, 129, 73	↑	1.6	Fatty acid metabolism	7.2	8.02E-05	6.79E-04	7.45E-04

[a] Change trend of relative amounts of the Tat group compared to the inaTat group. (↑): up-regulated. (↓): down-regulated. [b] The fold change of relative amounts of the Tat group compared to the inaTat group. [c] BCAA: branched-chain amino acid. [d] Variation of the metabolites concentrations in QC samples expressed as relative standard deviation (%RSD).

Table 3. Identification of differentiating metabolic features detected by using LC-MS and their metabolic pathways

no.	tr/min		m/z	formula	metabolites identified	trend [a]	fold change[b]	related pathway	%RSD[d]	*p*	*q*	*p*
	RP	HILIC	observed						(RP/HILIC)	(ANOVA)	(ANOVA)	(Tat/inaTat)
intracellular												
1	n.s.[e]	4.59	114.066	$C_4H_7N_3O$	Creatinine[h]	↑	2.3	Creatine metabolism	6.4	8.40E-04	7.43E-03	1.31E-03
2	1.29	15.19	132.102	$C_6H_{13}NO_2$	Isoleucine[g]	↓	0.4	BCAA[c] metabolism	10.7 / 5.8	7.80E-04	7.43E-03	1.49E-03
3	1.96	15.18	166.086	$C_9H_{11}NO_2$	Phenylalanine[g]	↑	2.2	Phenylalanine metabolism	11.2/4.9	9.60E-04	7.96E-03	1.64E-03
4	n.s.	13.15	137.071	$C_7H_8N_2O$	N-methylnicotinamide[h]	↑	1.7	Tryptophan metabolism	5.6	6.15E-04	6.62E-03	7.76E-04
5	3.74	14.68	205.097	$C_{11}H_{12}N_2O_2$	Tryptophan[g]	↓	0.6	Tryptophan metabolism	6.2 / 5.3	8.16E-05	4.92E-03	4.92E-04
6	n.s.	16.72	116.071	$C_5H_9NO_2$	Proline[g]	↑	4.6	Proline metabolism	4.7	9.78E-04	7.96E-03	3.61E-03
7	n.s.	19.54	132.077	$C_4H_9N_3O_2$	Creatine[h]	↓	0.5	Arginine and proline metabolism	5.4	5.84E-04	6.38E-03	6.93E-04
8	13.98	n.s.	300.289	$C_{18}H_{37}NO_2$	Sphingosine[h]	↑	1.5	Sphingolipid metabolism	4	6.15E-06	8.11E-04	8.74E-06
9	15.46	3.95	302.306	$C_{18}H_{39}NO_2$	Sphinganine[g]	↑	1.7	Sphingolipid metabolism	3.4/5.7	7.82E-07	3.09E-04	6.46E-06
10	17.71	25.09	496.339	$C_{24}H_{50}NO_7P$	LPC[f](16:0)[g]	↑	4.8	Phospholipid metabolism	6.7/8.2	1.82E-06	3.60E-04	3.48E-05
11	17.82	24.64	522.355	$C_{26}H_{52}NO_7P$	LPC(18:1)[h]	↑	1.7	Phospholipid metabolism	8.5/7.9	7.70E-04	7.43E-03	1.41E-03
12	19.71	24.48	524.370	$C_{26}H_{54}NO_7P$	LPC(18:0)[g]	↑	3.3	Phospholipid metabolism	4.8 / 3.8	3.87E-09	6.13E-06	7.19E-09
13	21.79	2.92	484.472	$C_{30}H_{61}NO_3$	Cer[i](d18:0/12:0)[h]	↑	4.3	Sphingolipid metabolism	6.8/5.4	1.68E-05	1.77E-03	3.56E-05
14	n.s.	22.51	703.575	$C_{39}H_{79}N_2O_6P$	Sphingomyelin (d18:1/16:0)[h]	↓	0.4	Sphingolipid metabolism	6.6	8.40E-04	7.43E-03	1.11E-03
15	22.66	n.s.	283.263	$C_{18}H_{34}O_2$	Oleic acid[h]	↑	1.9	Fatty acid metabolism	7.3	9.80E-04	7.96E-03	6.73E-03
16	22.42	2.39	512.503	$C_{32}H_{65}NO_3$	Cer(d18:0/14:0)[h]	↑	2.7	Sphingolipid metabolism	9.3/9.9	1.01E-07	5.33E-05	3.16E-06
17	n.s.	14.96	232.154	$C_{11}H_{21}NO_4$	Isobutyrylcarnitine[h]	↓	0.6	Fatty acid transportation	7.9	3.20E-06	5.41E-04	4.19E-05
18	n.s.	15.6	218.139	$C_{10}H_{19}NO_4$	Propionyl-L-carnitine[h]	↓	0.5	Fatty acid transportation	6.2	1.56E-03	9.41E-03	1.27E-02
19	n.s	17.44	162.113	$C_7H_{15}NO_3$	Carnitine[h]	↓	0.4	Fatty acid transportation	6.5	1.44E-06	3.60E-04	1.09E-05

20	n.s	18.25	758.570	$C_{42}H_{80}NO_8P$	Phosphatidylcholine(16:0/18:2)[h]	↓	0.6	Phospholipid metabolism	5.8	8.40E-04	7.43E-03	7.23E-03
21	n.s	18.71	706.539	$C_{38}H_{76}NO_8P$	Phosphatidylcholine(16:0/14:0)[h]	↓	0.5	Phospholipid metabolism	7.6	5.18E-06	7.45E-04	1.07E-05
extracellular												
1	1.28	15.18	132.102	$C_6H_{13}NO_2$	Isoleucine[g]	↓	0.6	BCAA metabolism	11.6/5.2	2.54E-06	4.94E-04	1.89E-05
2	1.94	15.17	166.086	$C_9H_{11}NO_2$	Phenylalanine[g]	↑	1.6	Phenylalanine metabolism	9.4/4.5	3.80E-04	1.82E-03	1.19E-03
3	13.55	n.s.	274.275	$C_{16}H_{35}NO_2$	C16 Sphinganine[h]	↑	1.8	Sphingolipid metabolism	5.9	5.78E-07	1.87E-04	7.75E-07
4	13.69	5.83	318.301	$C_{18}H_{39}NO_3$	Phytosphingosine[h]	↑	1.7	Sphingolipid metabolism	7.6/8.8	9.21E-10	8.96E-07	3.68E-09
5	13.96	n.s.	300.290	$C_{18}H_{37}NO_2$	Sphingosine[h]	↑	2.0	Sphingolipid metabolism	6.2	6.72E-06	9.10E-04	9.27E-05
6	15.42	3.97	302.305	$C_{18}H_{39}NO_2$	Sphinganine[g]	↑	2.1	Sphingolipid metabolism	3.7 / 6.7	1.05E-07	5.11E-05	2.78E-07
7	17.71	25.08	496.339	$C_{24}H_{50}NO_7P$	LPC(16:0)[g]	↑	2.8	Phospholipid metabolism	4.0/7.8	4.98E-05	1.04E-03	7.89E-05
8	17.81	24.62	522.355	$C_{26}H_{52}NO_7P$	LPC(18:1)[h]	↑	1.9	Phospholipid metabolism	4.4/6.8	9.82E-07	2.39E-04	3.68E-06
9	19.69	24.47	524.370	$C_{26}H_{54}NO_7P$	LPC(18:0)[g]	↑	2.6	Phospholipid metabolism	6.7/7.5	7.48E-06	9.10E-04	2.15E-05
10	21.77	2.91	484.472	$C_{30}H_{61}NO_3$	Cer(d18:0/12:0)[h]	↑	2	Sphingolipid metabolism	4.8/7.9	7.20E-04	2.96E-03	1.02E-03
11	22.41	2.38	512.503	$C_{32}H_{65}NO_3$	Cer(d18:0/14:0)[h]	↑	1.9	Sphingolipid metabolism	6.8/7.6	9.52E-05	1.04E-03	6.45E-04
12	22.67	n.s.	283.263	$C_{18}H_{34}O_2$	Oleic acid[h]	↑	2.7	Fatty acid metabolism	6.1	3.12E-06	5.06E-04	1.99E-05

[a] Change trend of relative amounts of the Tat group compared to the inaTat group. (↑): up-regulated. (↓): down-regulated. [b] The fold change of relative amounts of the Tat group compared to the inaTat group. [c] BCAA: branched-chain amino acid. [d] Variation of the metabolites concentrations in QC samples expressed as relative standard deviation (%RSD). [e] n. s.: no signal. [f] LPC: Lysophosphatidylcholine. [i] Cer: Ceramide. [g] Metabolites validated with standard sample. [h] Metabolites putatively annotated.

Table 4. Result from metabolic pathway analysis with MetaboAnalyst 2.0[a]

no.	pathway name	total cmpd	hits	raw p	-log(p)	impact
1	Sphingolipid metabolism	25	5	8.00E-06	11.736	0.2404
2	Glycine, serine and threonine metabolism	48	3	7.46E-06	11.807	0.1885
3	Pyruvate metabolism	32	2	5.34E-05	9.838	0.1376
4	Inositol phosphate metabolism	39	2	8.74E-06	11.647	0.1370
5	Arginine and proline metabolism	77	2	7.08E-06	11.858	0.1339
6	Citrate cycle	20	3	6.81E-06	11.897	0.1213
7	Phenylalanine metabolism	45	3	1.47E-05	11.127	0.1191
8	Tryptophan metabolism	79	1	2.18E-05	10.732	0.1085
9	Pentose phosphate pathway	32	2	6.45E-06	11.952	0.1053
10	Glycerophospholipid metabolism	39	2	2.83E-05	10.474	0.1037
11	Glycolysis or Gluconeogenesis	31	3	7.33E-06	11.823	0.1008

[a]Total is the total number of compounds in the pathway; the hits is the actually matched number from the user uploaded data; the raw p is the original p value calculated from the enrichment analysis; the impact is the pathway impact value calculated from pathway topology analysis.

Figure legends:

Figure 1. Schematic flowchart of the metabolic profiling strategy used in this study. Bioactivities of Tat protein were evaluated by MTT assay and apoptosis assay. Jurkat cells were treated with bioactive Tat protein, inaTat or PBS. Intracellular and extracellular metabolites were extracted and analyzed by LC-MS and GC-MS. Multivariate statistics was applied to extract meaningful information in the complex GC-MS and LC-MS spectral data. Compounds with significant contribution to the variation of metabolic profiles between Tat-treated and inaTat groups were identified and further verified by reference compounds available. Metabolite-related enzymes were determined by real-time PCR.

Figure 2. (A) Cell proliferation evaluated by MTT assays. 10^5 Jurkat T-cells were incubated with PBS, Tat or inaTat protein. Inhibition on cell growth was calculated based on the absorbance at 570 nm. The error bars represent the standard deviation (S.D.) measured in three independent experiments carried out in five replicates. *$p<0.05$, compared with inaTat group. (B) Apoptosis assay using Jurkat T-cells. The percentage of annexin-stained apoptotic cells was analyzed by flow cytometry and is summarized in a histogram (C). The error bars represent the S.D. measured in three independent experiments carried out in triplicate. *$p<0.05$, compared with inaTat and control groups.

Figure 3. Typical total ions current chromatograms (TICs) from intracellular samples separated on GC (A), RPLC (B) and HILIC (C); extracellular samples separated on GC (D), RPLC (E) and HILIC (F). (G) Extracted ion chromatograms for *m/z* 302.306 from intracellular samples of the control, inaTat and Tat treated Jurkat cells separated on RPLC.

Figure 4. PCA of GC-MS spectra from intracellular metabolites in Jurkat cells (A), PCA of LC-MS spectra from intracellular metabolites (B), PCA of GC-MS spectra from extracellular metabolites (C) and PCA of LC-MS spectra from extracellular metabolites (D). (■) control group, (▲) inaTat group and (◆) Tat group.

Figure 5. Summary of pathway analysis with MetaboAnalyst 2.0. a, sphingolipid metabolism; b, glycine, serine and threonine metabolism; c, pyruvate metabolism; d, inositol phosphate metabolism; e, arginine and proline metabolism; f, citrate cycle; g, phenylalanine metabolism; h, tryptophan metabolism; i, pentose phosphate pathway; j, glycerophospholipid metabolism; k, glycolysis or gluconeogenesis.

Figure 6. Schematic overview of the metabolites and major metabolic pathways as well as pathway-related enzyme changes in Tat-treated Jurkat cells. The metabolites and enzymes (italic) are shown in color: red represents

increased metabolites or enzymes, green represents decreased metabolites or enzymes, yellow represents no change, and the open circles represent no detected metabolites.

Figure 7. Real-time quantitative PCR was performed for relative quantization of target mRNA on each sample using the $2^{-\Delta\Delta CT}$ method. The assay showed fold changes of target mRNA in Tat- and inaTat-treated cells relative to that in control cells. The experiment was repeated for three times and the data were obtained by average. The error bars represent the S.D. of the mean. *$p < 0.05$, compared with inaTat and control groups. Key: LDHA, lactate dehydrogenase A; SDHB, succinate dehydrogenase B; MDH, malate dehydrogenase; SPT, serine palmitoyltransferase; ASM, acid sphingomyelinases; PLA1A, phospholipase A1 member A; PLA2G4C, phospholipase A2 group IVC; IDO, indoleamine-2,3-dioxygenase.

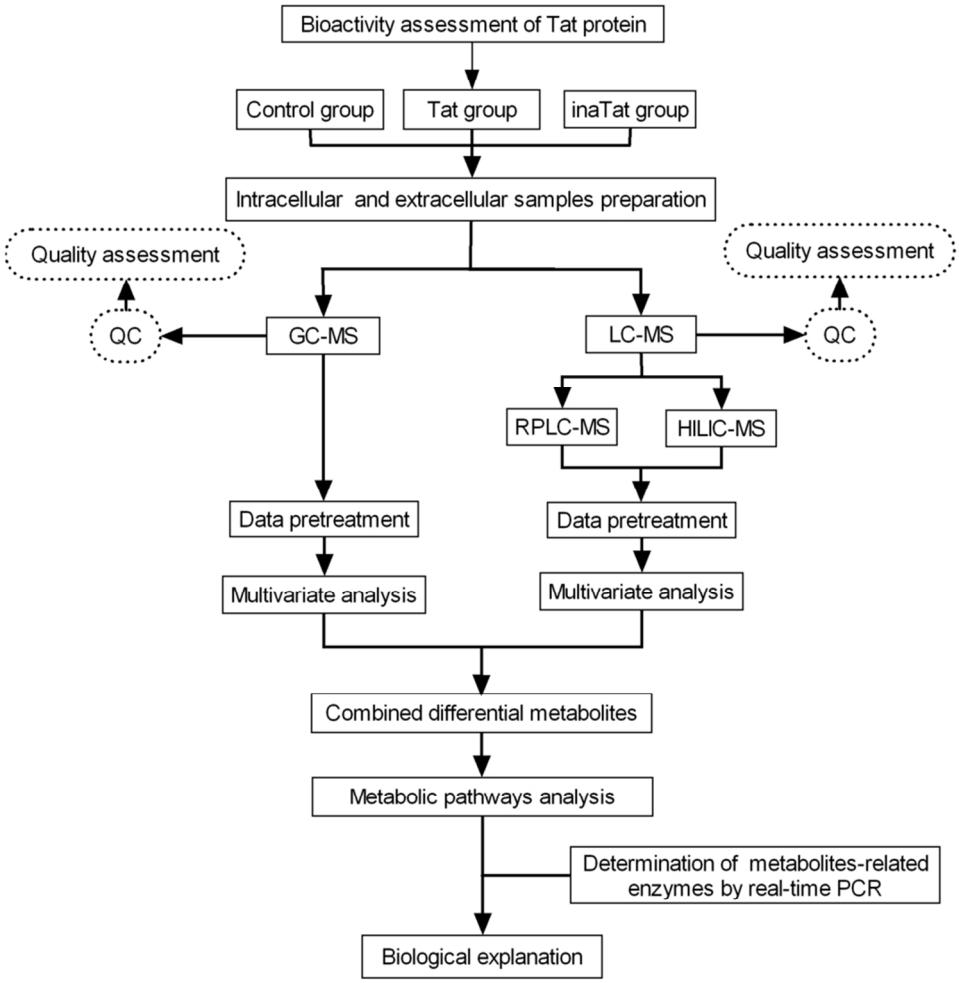

Figure 1. Schematic flowchart of the metabolic profiling strategy used in this study. Bioactivities of Tat protein were evaluated by MTT assay and apoptosis assay. Jurkat cells were treated with bioactive Tat protein, inaTat or PBS. Intracellular and extracellular metabolites were extracted and analyzed by LC-MS and GC-MS. Multivariate statistics was applied to extract meaningful information in the complex GC-MS and LC-MS spectral data. Compounds with significant contribution to the variation of metabolic profiles between Tat-treated and inaTat groups were identified and further verified by reference compounds available. Metabolite-related enzymes were determined by real-time PCR.
44x45mm (600 x 600 DPI)

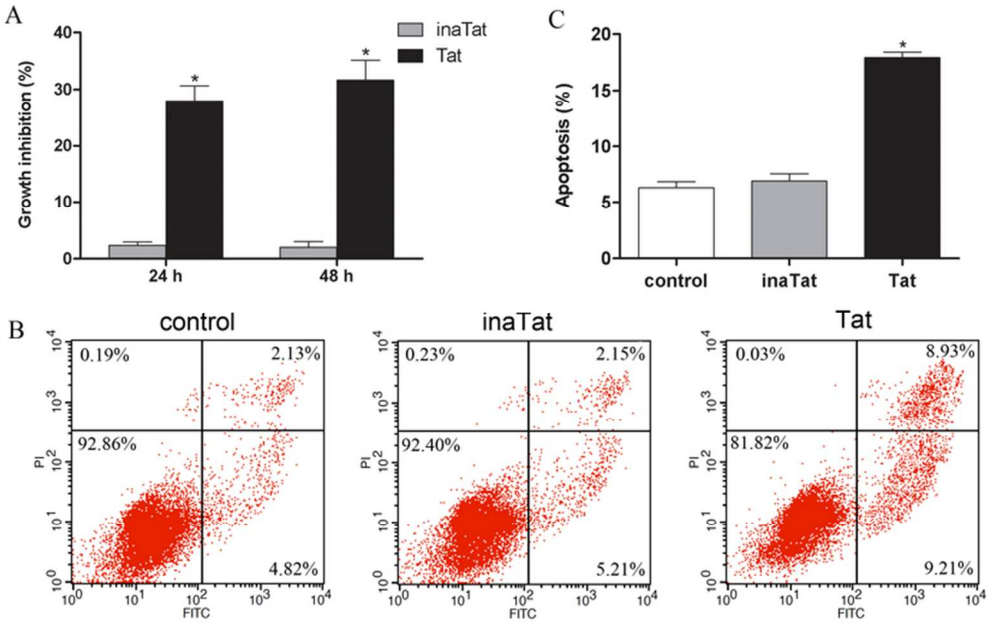

Figure 2. (A) Cell proliferation evaluated by MTT assays. 105 Jurkat T-cells were incubated with PBS, Tat or inaTat protein. Inhibition on cell growth was calculated based on the absorbance at 570 nm. The error bars represent the standard deviation (S.D.) measured in three independent experiments carried out in five replicates. *p<0.05, compared with inaTat group. (B) Apoptosis assay using Jurkat T-cells. The percentage of annexin-stained apoptotic cells was analyzed by flow cytometry and is summarized in a histogram (C). The error bars represent the S.D. measured in three independent experiments carried out in triplicate. *p<0.05, compared with inaTat and control groups.
35x22mm (600 x 600 DPI)

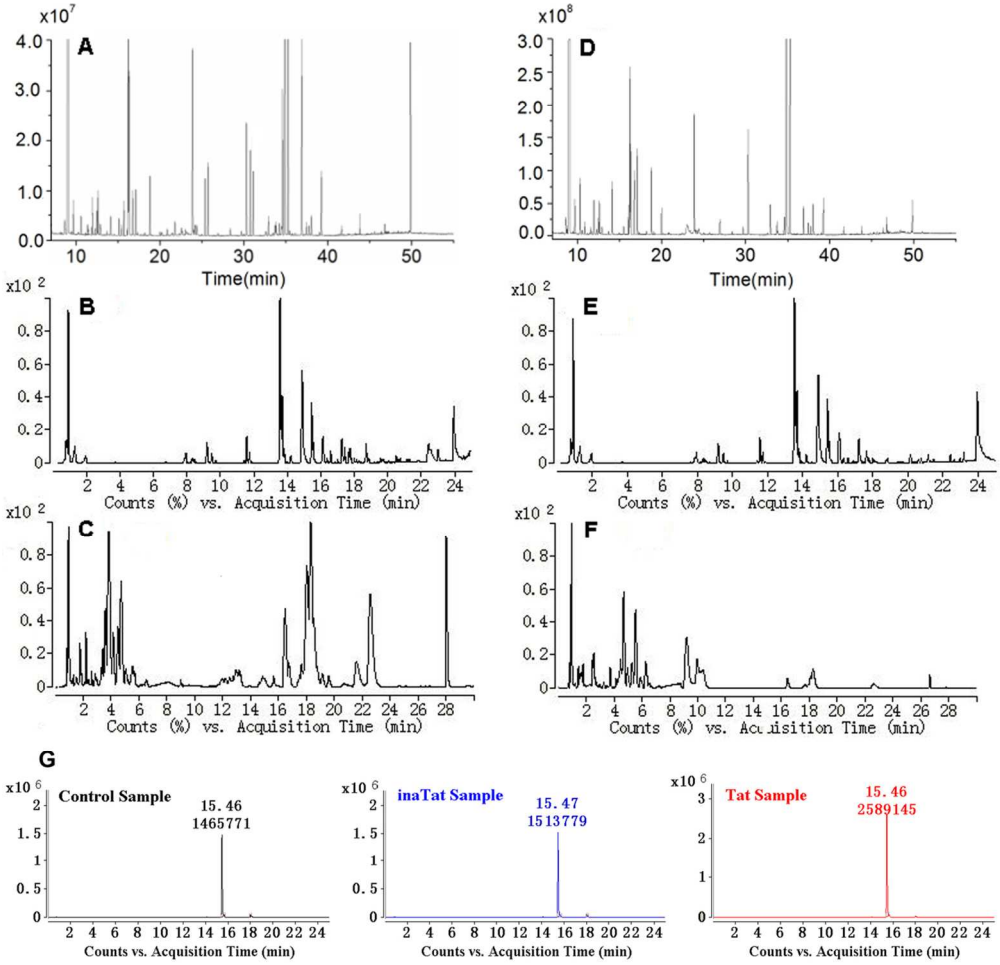

Figure 3. Typical total ions current chromatograms (TICs) from intracellular samples separated on GC (A), RPLC (B) and HILIC (C); extracellular samples separated on GC (D), RPLC (E) and HILIC (F). (G) Extracted ion chromatograms for m/z 302.306 from intracellular samples of the control, inaTat and Tat treated Jurkat cells separated on RPLC.
60x58mm (600 x 600 DPI)

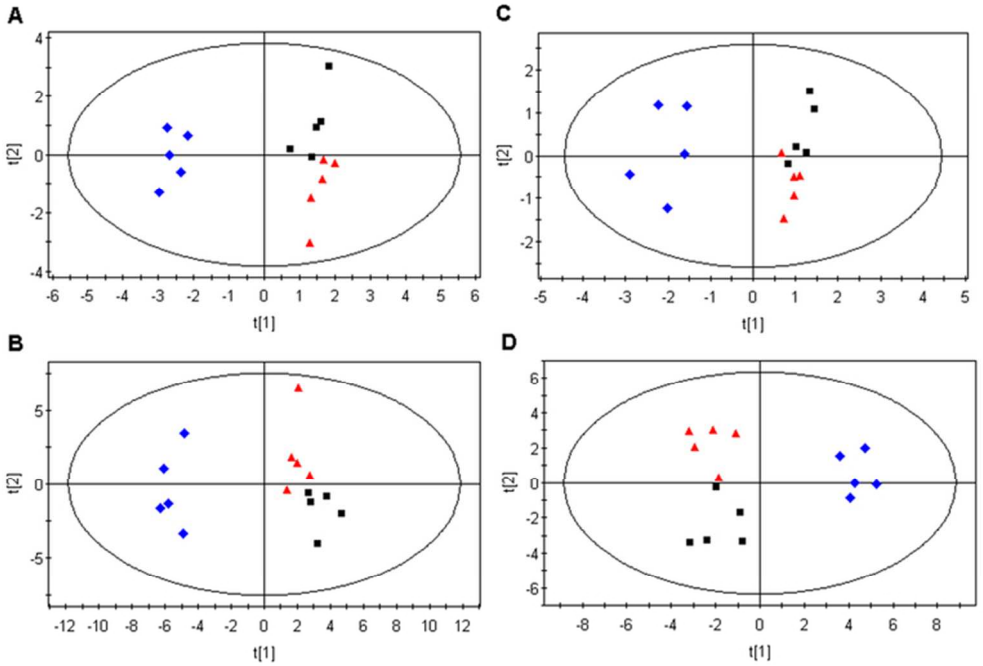

Figure 4. PCA of GC-MS spectra from intracellular metabolites in Jurkat cells (A), PCA of LC-MS spectra from intracellular metabolites (B), PCA of GC-MS spectra from extracellular metabolites (C) and PCA of GC-MS spectra from extracellular metabolites (D). (■) control group, (▲) inaTat group and (◆) Tat group.
32x22mm (600 x 600 DPI)

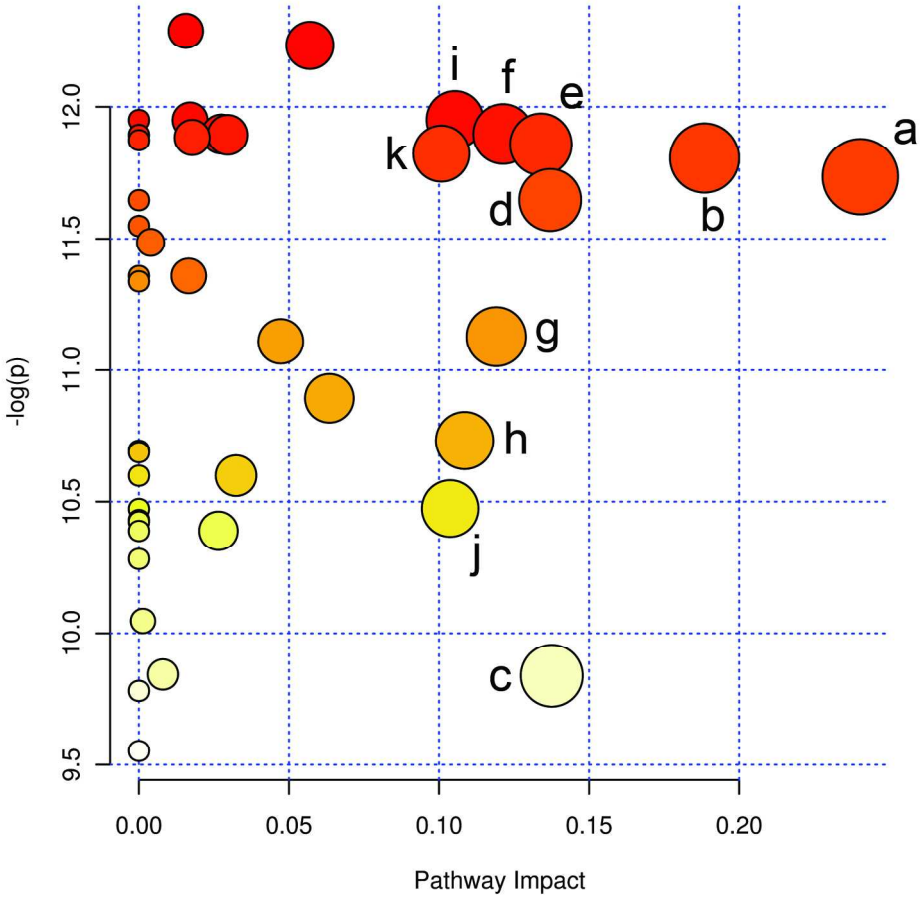

Figure 5. Summary of pathway analysis with MetaboAnalyst 2.0. a, sphingolipid metabolism; b, glycine, serine and threonine metabolism; c, pyruvate metabolism; d, inositol phosphate metabolism; e, arginine and proline metabolism; f, citrate cycle; g, phenylalanine metabolism; h, tryptophan metabolism; i, pentose phosphate pathway; j, glycerophospholipid metabolism; k, glycolysis or gluconeogenesis.
182x182mm (300 x 300 DPI)

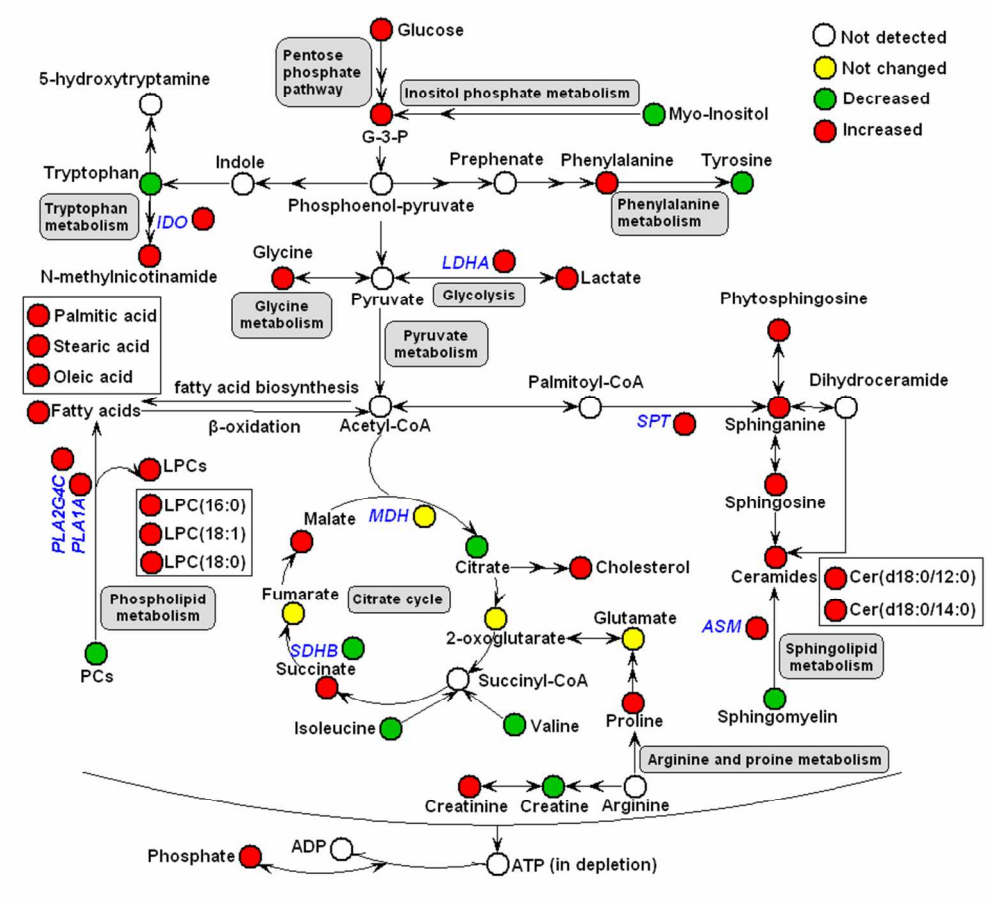

Figure 6. Schematic overview of the metabolites and major metabolic pathways as well as pathway-related enzyme changes in Tat-treated Jurkat cells. The metabolites and enzymes (italic) are shown in color: red represents increased metabolites or enzymes, green represents decreased metabolites or enzymes, yellow represents no change, and the open circles represent no detected metabolites.
80x72mm (300 x 300 DPI)

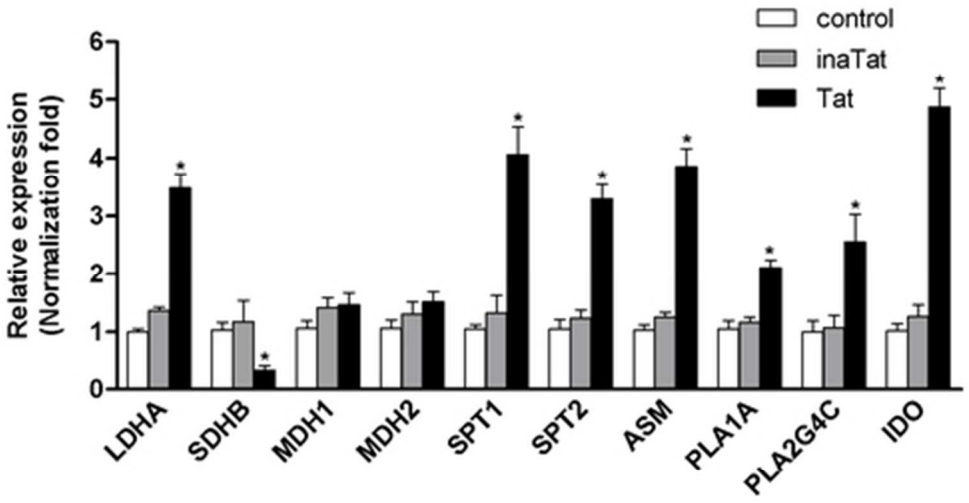

Figure 7. Real-time quantitative PCR was performed for relative quantization of target mRNA on each sample using the 2−ΔΔCT method. The assay showed fold changes of target mRNA in Tat- and inaTat-treated cells relative to that in control cells. The experiment was repeated for three times and the data were obtained by average. The error bars represent the S.D. of the mean. *p < 0.05, compared with inaTat and control groups. Key: LDHA, lactate dehydrogenase A; SDHB, succinate dehydrogenase B; MDH, malate dehydrogenase; SPT, serine palmitoyltransferase; ASM, acid sphingomyelinases; PLA1A, phospholipase A1 member A; PLA2G4C, phospholipase A2 group IVC; IDO, indoleamine-2,3-dioxygenase.
21x12mm (600 x 600 DPI)

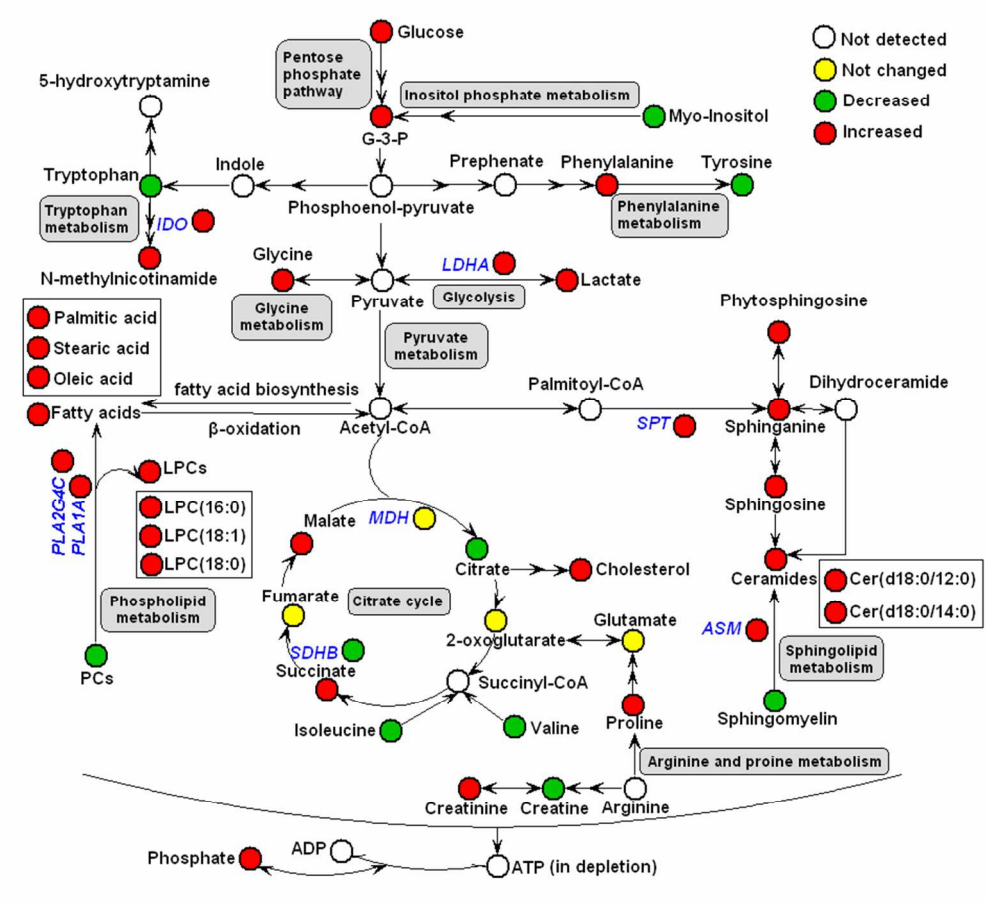

Graphical Abstract
80x72mm (300 x 300 DPI)